Supporting Information for

Enhanced photocatalytic hydrogen evolution *via* optimization of interfacial energy and mass flows

Chunyang Zhang,[a†] Shidong Zhao,[a†] Shujian Wang,*[a†] Jie Huang,[a] Biao Wang,[a] Kejian Lu,[a] Rui Zhao, [a] Rui Song,*[a,c] Maochang Liu*[a,b]

[a]International Research Center for Renewable Energy, State Key Laboratory of Multiphase Flow in Power Engineering, School of Energy and Power Engineering, Xi'an Jiaotong University, Xi'an, Shaanxi 710049, P. R. China

[b]Suzhou Academy of Xi'an Jiaotong University, Suzhou, Jiangsu 215123, P. R. China

[c]Solar Fuels Group, Department of Chemistry, University of Toronto, 80 St. George Street, Toronto, Ontario M5S 3H6, Canada.

[†]C.Z., S.Z. and S.W. contributed equally to this work.

*Corresponding authors: wangshj@stu.xjtu.edu.cn (S. W.), ruisong.song@mail.utoronto.ca (R. S.), maochangliu@mail.xjtu.edu.cn (M. L.)

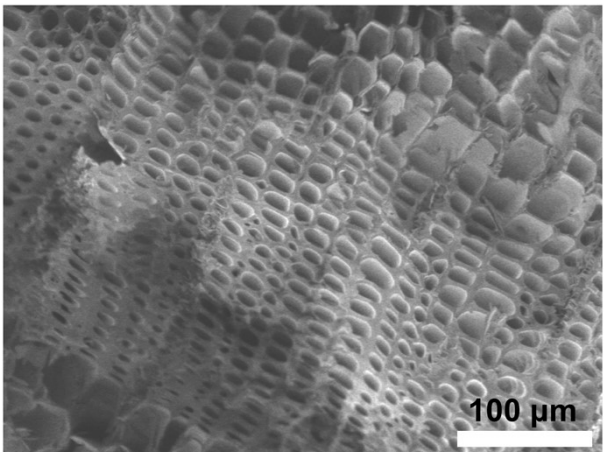

Fig S1. Cross-sectional SEM image of CW.

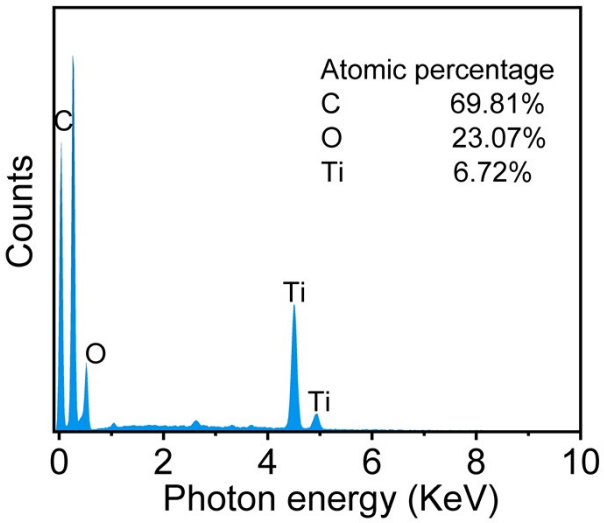

Fig. S2. EDX spectrum of T/CW.

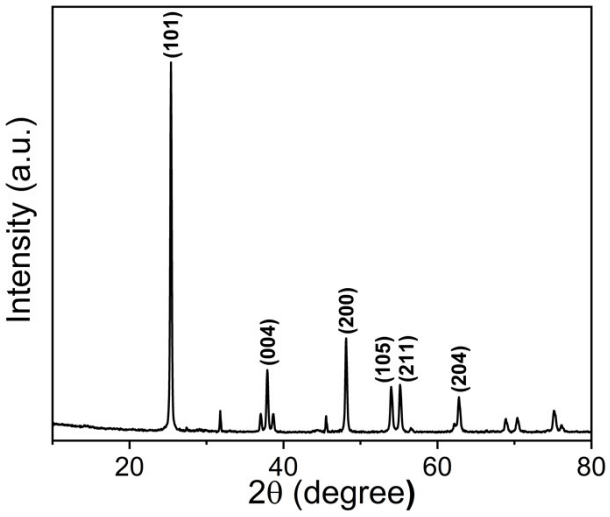

Fig S3. XRD pattern of TiO_2.

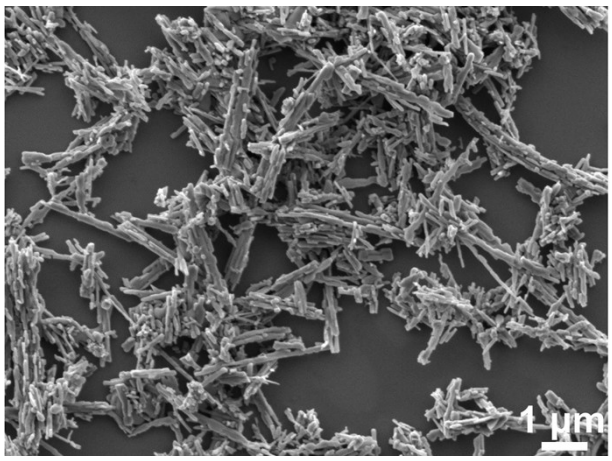

Fig S4. SEM image of TiO_2.

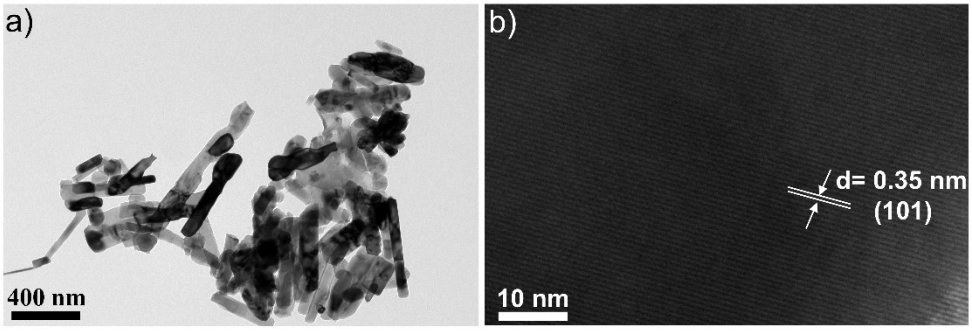

Fig S5. TEM images of TiO_2. (a) TEM and (b)HRTEM.

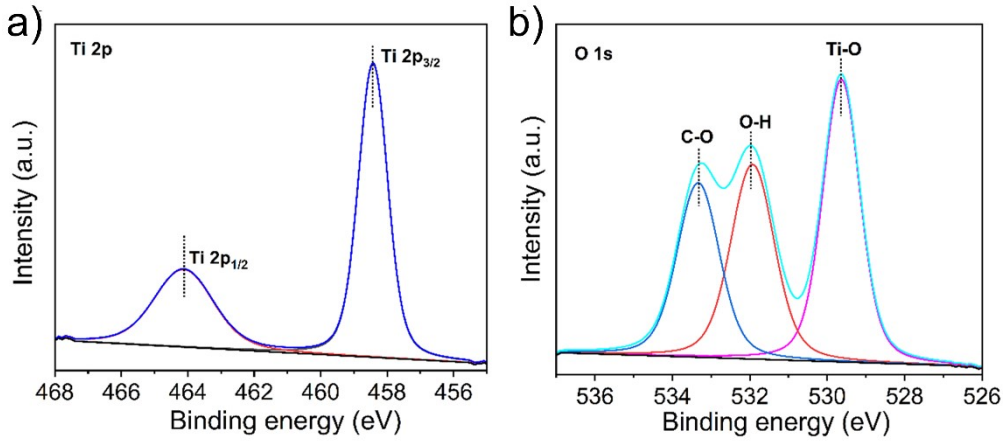

Fig S6. The high-resolution XPS spectras of (a) Ti and (b) O1s.

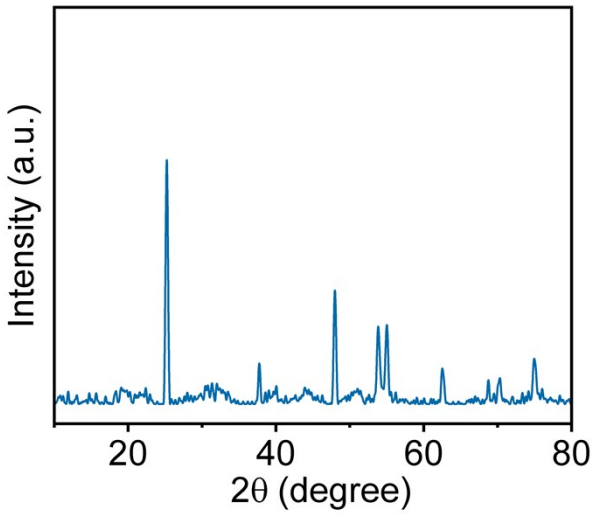

Fig. S7. XRD pattern of the TiO_2 with a Pt loading of 1.0 wt%.

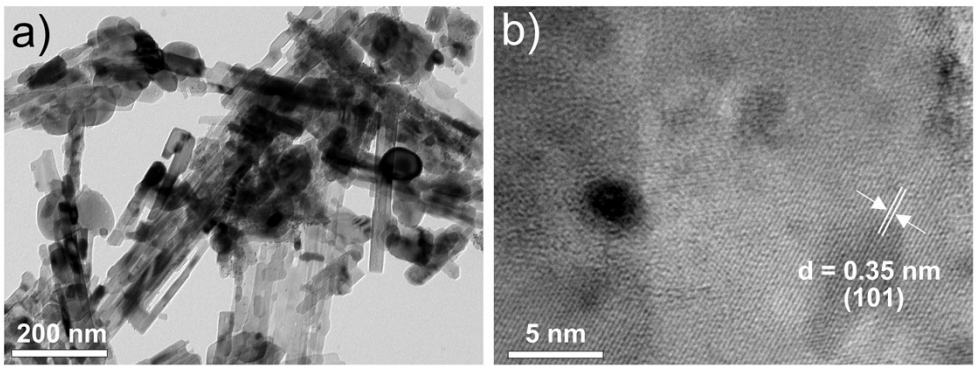

Fig. S8. TEM and HRTEM images of the TiO_2 with a Pt loading of 1.0 wt%. (a) TEM. (b) HRTEM.

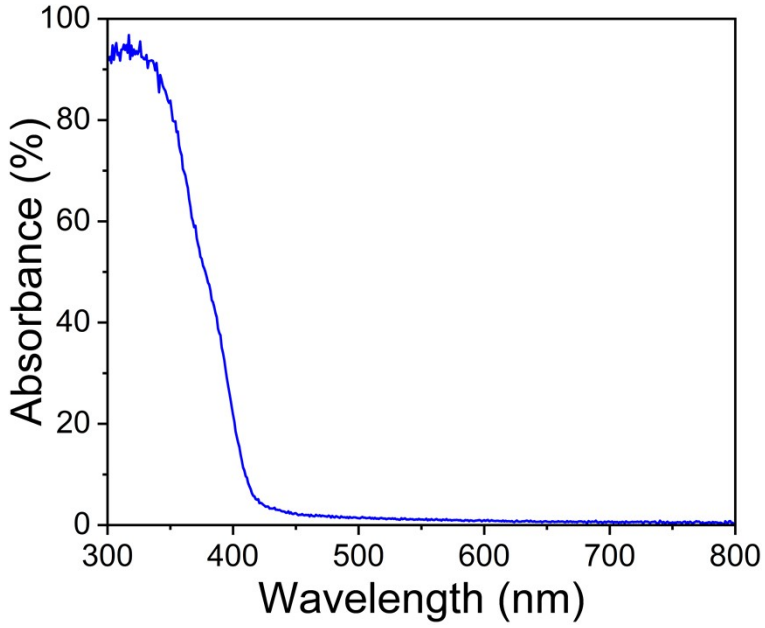

Fig S9. UV-vis diffuse-reflectance spectra of TiO_2.

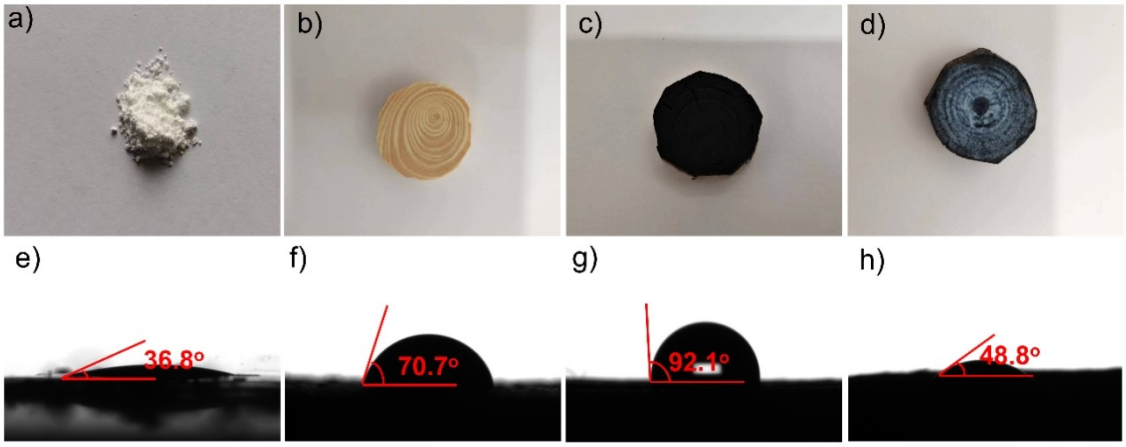

Fig S10. (a-d) photos of the TiO_2, Wood, CW and T/CW. (e-h) The contact angle measurement of TiO_2, Wood, CW and T/CW.

Fig S11. Photo of T/C-W floating on liquid water.

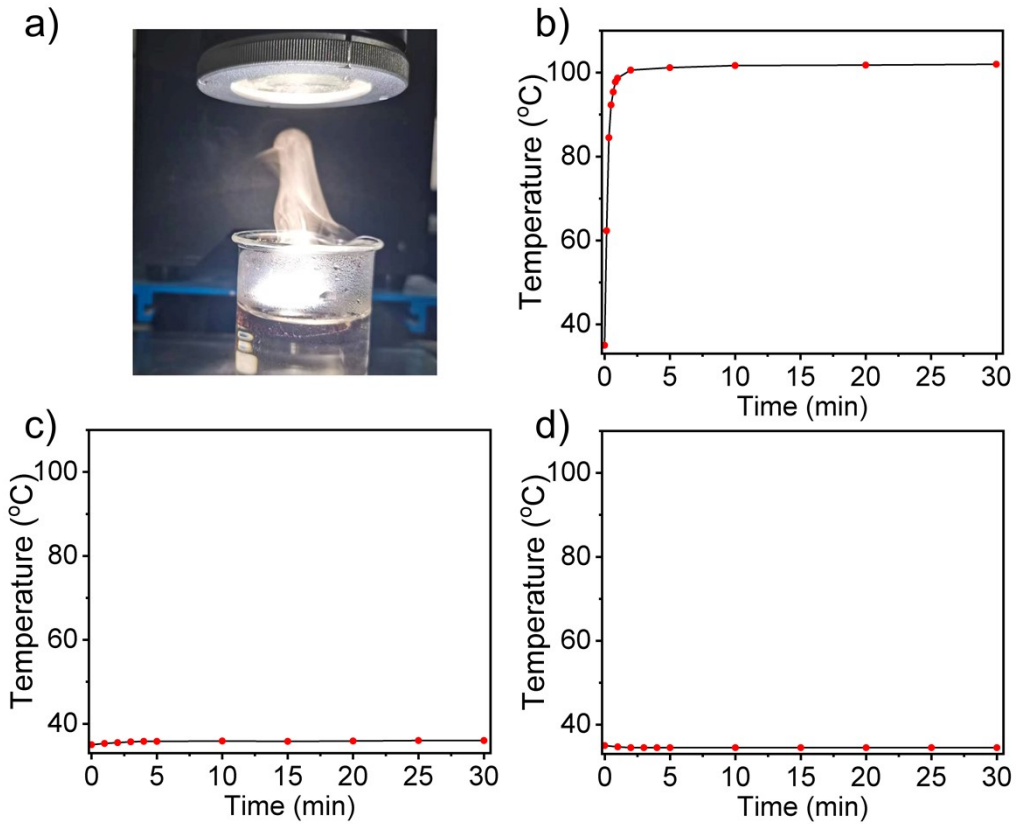

Fig. S12. (a) Photo of steam generation of the biphasic T/CW system under solar irradiation. (b) T/CW surface temperature as a function of time. (c) Water temperature as a function of time without T/CW. (d) Water temperature as a function of time with T/CW.

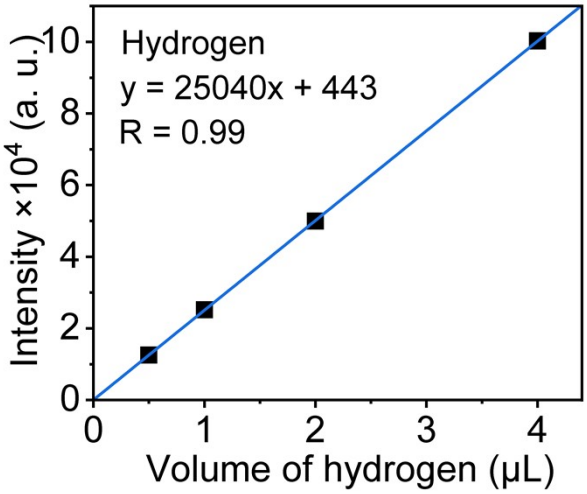

Fig. S13. High performance Gas chromatography (GC) quantitative curve of hydrogen samples.

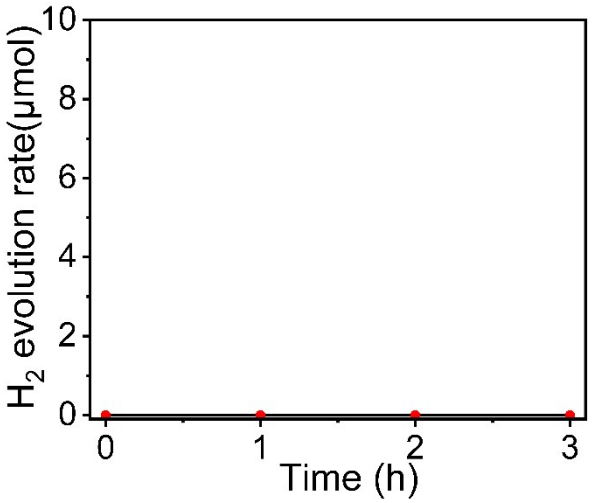

Fig S14. Time-dependent photocatalytic H_2 evolution of T/CW system without solar irradiation.

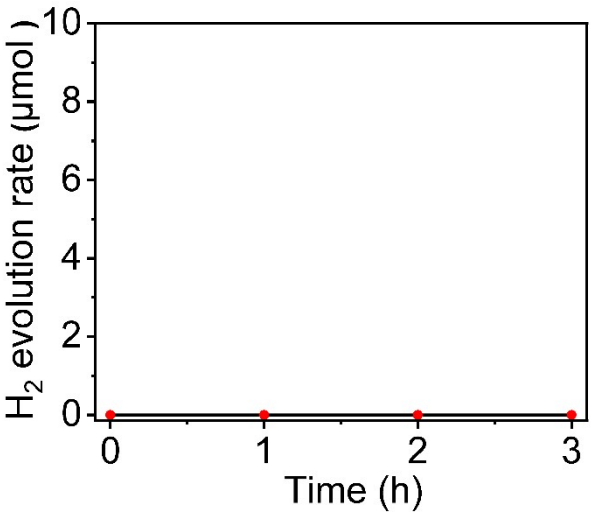

Fig S15. Time-dependent photocatalytic H_2 evolution of CW system without photocatalyst.

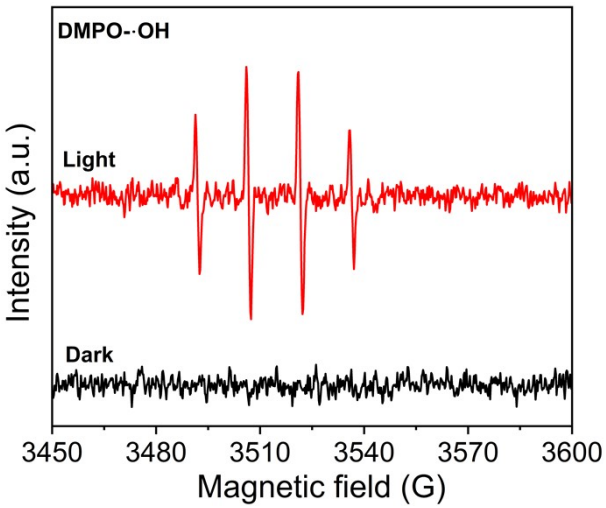

Fig S16. ESR spectra for identifying DMPO-•OH under dark and solar irradiation.

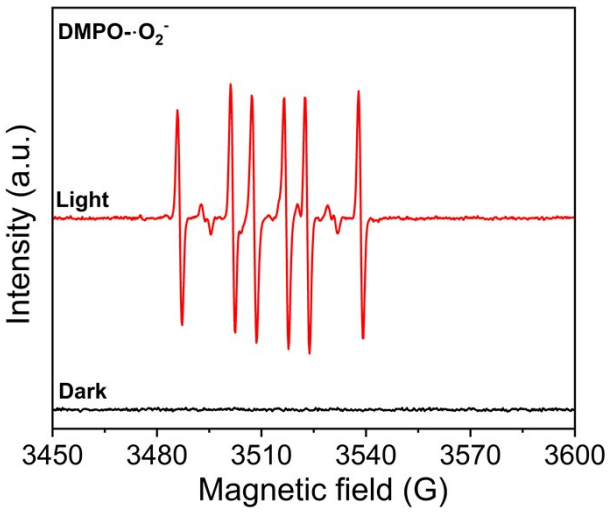

Fig S17. ESR spectra for identifying DMPO-•O_2^- under dark and solar irradiation.

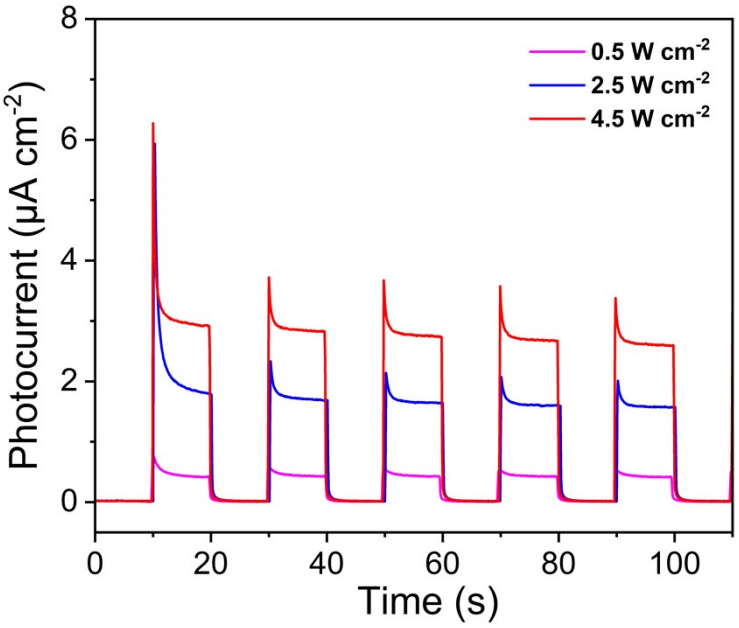

Fig S18. Photocurrent responses curves of TiO_2 under different solar intensity.

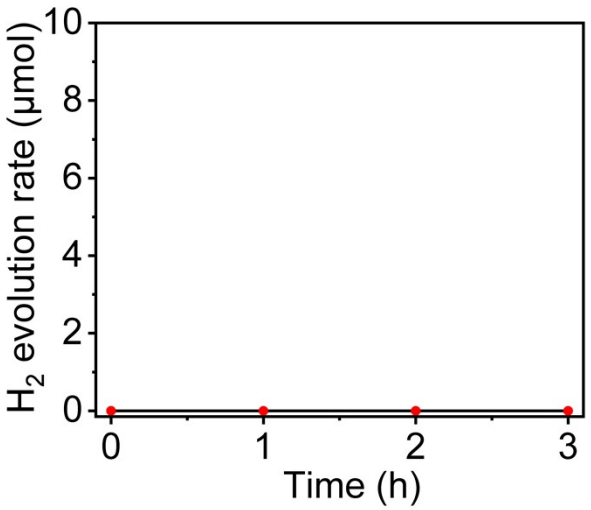

Fig. S19. Photocatalytic H_2 evolution performance of the T/CW system under 95°C and dark conditions.

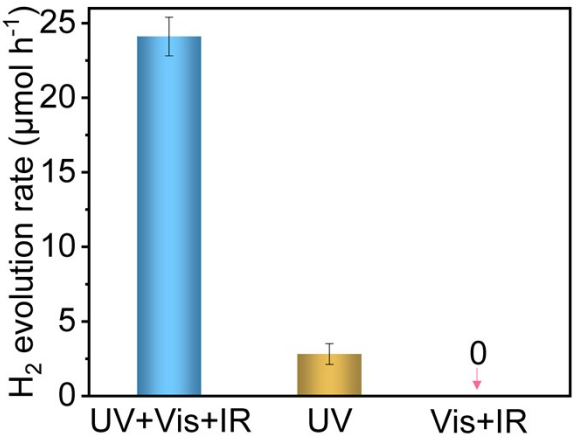

Fig. S20. Photocatalytic H_2 evolution performance of the T/CW system under full-spectrum(UV+Vis+IR), ultraviolet (UV), and visible-infrared (Vis+IR) light. Bars show the mean of three independent experiments, with error bars representing the range (min to max).

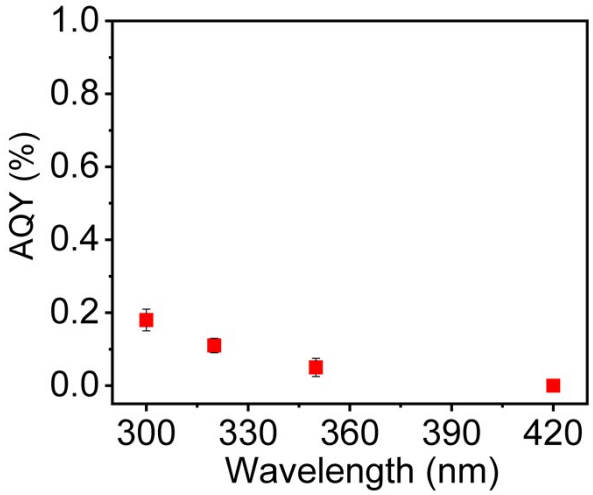

Fig. S21. Wavelength-dependent apparent quantum yield (AQY) for photocatalytic water splitting for the T/CW system.

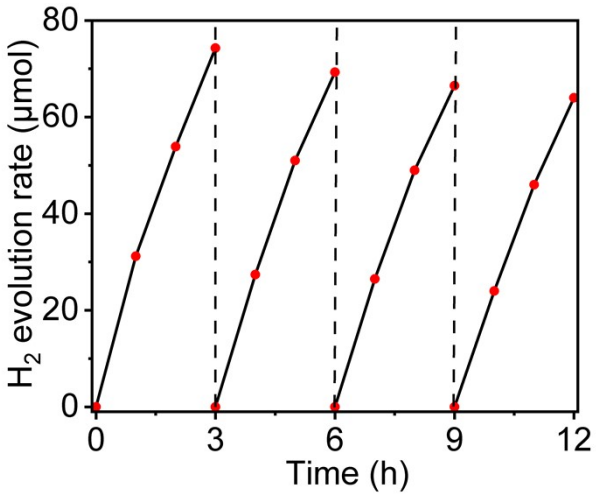

Fig. S22. Time-dependent photocatalytic H_2 evolution of T/CW system with simulated seawater.

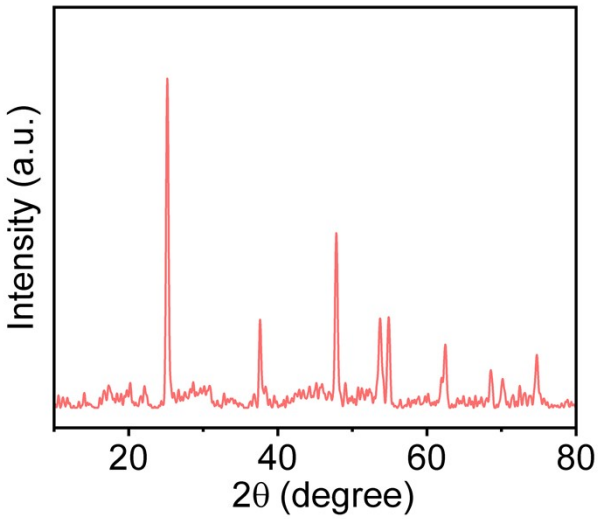

Fig. S23. XRD pattern of TiO_2 with a Pt loading of 1.0 wt% after 12 h of photocatalytic reaction in the biphasic system with simulated seawater.

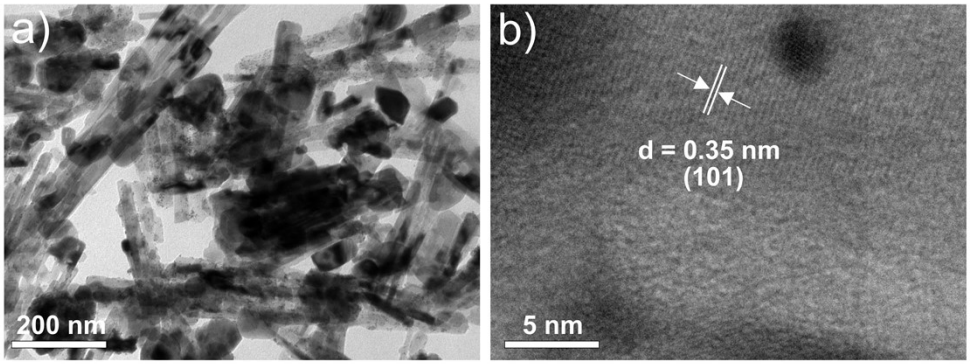

Fig. S24. TEM and HRTEM images of Pt-TiO_2 after 12 h of photocatalytic reaction in the biphasic system with simulated seawater. (a) TEM . (b) HRTEM.

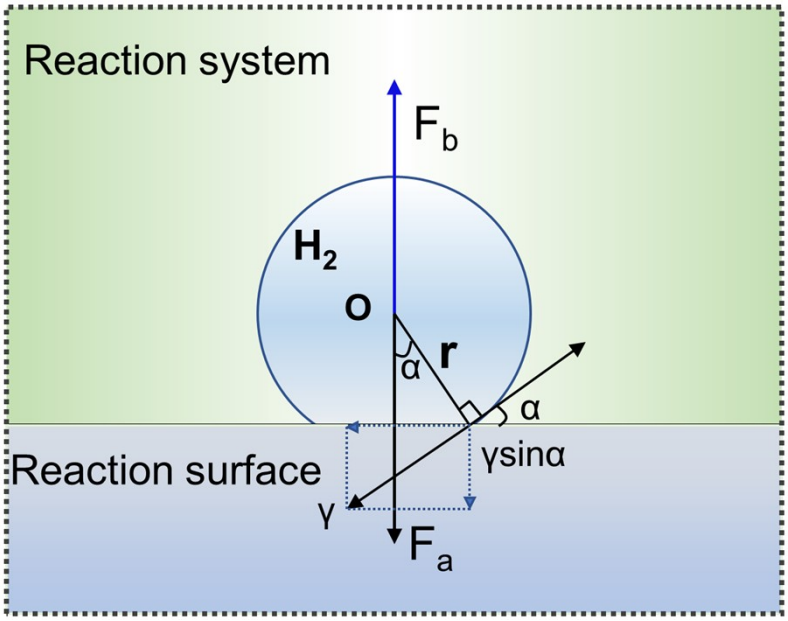

Fig S25. Force analysis of the bubble sticking on the reaction interface.

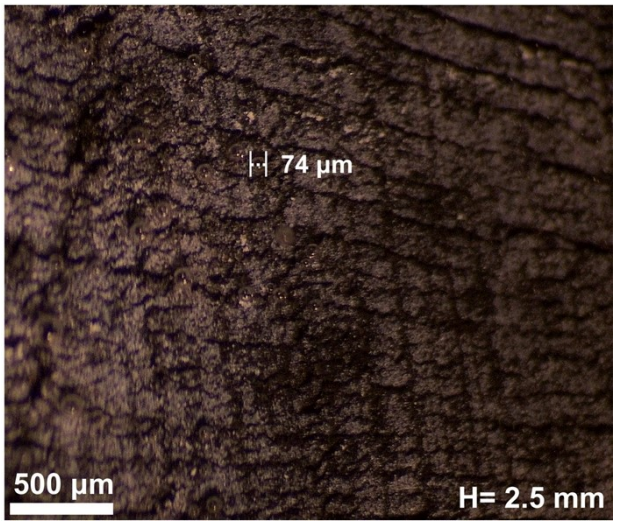

Fig S26. Photo of bubbles at the distance of 2.5 mm below water surface.

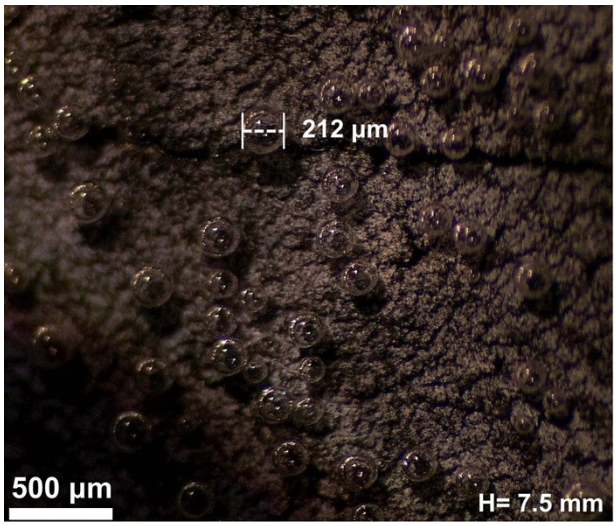

Fig S27. Photo of bubbles at the distance of 7.5 mm below water surface.